Study of Interannual Variability of the Winter Mesothermal Temperature Maximum Layer in Southern Baikal

Ilya Aslamov [1], Elena Troitskaya [1,*], Ruslan Gnatovsky [1], Inna Portyanskaya [1,2], Sergey Lovtsov [2], Yuri Bukin [1] and Nikolay Granin [1]

[1] Limnological Institute, Siberian Branch of Russian Academy of Sciences, 664033 Irkutsk, Russia; ilya_aslamov@bk.ru (I.A.); gnat@lin.irk.ru (R.G.); iportyanskaya@mail.ru (I.P.); bukinyura@mail.ru (Y.B.); granin.n@gmail.com (N.G.)

[2] Department of Theoretical Physics, Faculty of Physics, Irkutsk State University, 664003 Irkutsk, Russia; lsv@api.isu.ru

* Correspondence: elena.troitskaya@lin.irk.ru; Tel.: +7-(3952)425768

Abstract: This paper is devoted to the study of the mesothermal temperature maximum layer (MTML) in Lake Baikal, which is observed during the period of winter stratification. On the one hand, this is a rather well-known phenomenon; on the other hand, it is not sufficiently studied, although it has a significant impact on the thermal regime in winter and water dynamics during the periods of formation and breakdown of inverse temperature stratification. Our work presents the results of analyzing the spatial and temporal variability of the main MTML parameters and their dependence on hydrometeorological factors. For this purpose, CTD soundings and mooring data obtained in the western part of the southern basin of Lake Baikal in 2000–2022 were analyzed in comparison to ERA5-Land reanalysis. The MTML parameters have noticeable within-season and interannual spatial and temporal variability. This is obviously related to the influence of the processes of vertical turbulent mixing, internal wave action, and current patterns. The analysis of interannual differences revealed four types of behavior of the maximum MTML temperature during the ice season. The influence of wind conditions on the main MTML parameters (maximum MTML temperature, depth of its occurrence, and depth of the upper MTML boundary) was shown not only in the fall, but also in the summer period, when heat accumulation in the Baikal water column takes place. With the increased wind activity in the late fall, the MTML is formed deeper and has lower maximum temperature values. At lower wind activity in the fall, the MTML is closer to the surface and the values of the maximum MTML temperature are higher. A change in wind activity in the summer leads to the opposite effect. In spite of the essential trends over the study period in the dates of the occurrence of hydrological events, no noticeable trends were registered for the maximum MTML temperature, its depth, and the depth of the upper boundary of the MTML.

Keywords: Lake Baikal; mesothermal temperature maximum layer; water temperature; wind; ice cover duration

1. Introduction

Lake Baikal, located in Siberia, Russia, is the world's deepest and oldest freshwater lake. It has a maximum depth of approximately 1642 m [1] and is estimated to be around 25 million years old. It has a total volume of approximately 23,000 cubic kilometers, making it the world's largest freshwater lake by volume. Lake Baikal harbors an astonishing array of species (more than 2600 species of animals [2] and about 1400 species of aquatic plants [3], many of which are endemic (about 1500 species of animals [2] and around two thirds of the species of aquatic plants (personal comment by T.A. Shcherbakova)). Lake Baikal's unique hydrophysical conditions and ecological importance make it a remarkable natural marvel that continues to captivate scientists and visitors from around the world. It also was awarded World Heritage Site status by the UN in 1996.

Baikal is a deep dimictic lake of temperate latitudes; so, twice a year (May–June and November–December) it is subject to changes in temperature stratification. During periods of homothermy, water temperature in the active layer (0–250 m) is equalized at around 3.6 °C [4]. In late autumn, temperature equalization occurs due to strong wind mixing, in spring—by the development of under-ice temperature convection driven by radiation heating, and after ice-off—wind is also effected [4]. During winter, Lake Baikal experiences extreme temperatures due to its location in a region with a severe continental climate, air temperatures can plummet down to -20–-30 °C, and the lake freezes for 3–5 months in a year, forming a layer of ice that can be more than a meter thick. Ice cover insulates the water from the cold air, prevents significant heat loss from the lake, and it also excludes wind-driven mixing.

The large depths of Baikal cause a significant influence of the dependence of the temperature of the maximum density of water (T_{md}) on the hydrostatic pressure on the processes of vertical transport of matter and energy [5–8]. Thus, temperature dependence of the compressibility of water leads to a shift of the temperature of maximum density by 0.021 °C bar^{-1} (thermobaricity effect [9]).

Thermobaricity is the cause of deep-water renewal or "ventilation" in Lake Baikal. At temperatures of 3.5–3.7 °C the equalized active water layer (after the fall homothermy in November–December and before the spring homothermy in May), with increasing wind turbulence during these periods [10], conditions of thermobaric instability may arise, and deep convection develops with surface water intrusions into the deep and bottom zones of the lake [4–6,11–18]. This seasonal mixing of surface and deep waters is a vital part of the renewal process in Lake Baikal. Similar deep-water renewal has also been reported in other deep lakes: the Canadian lakes Kamloops (143 m), Babine (186 m) [19], and Great Slave Lake (564 m) [20]; Lake Crater (USA, 594 m) [21]; the Japanese lakes Towada (327 m) and Shikotsu (363 m) [22]; and others. A comprehensive review of processes that influence mixing and convection in lakes is given in [8].

The thermobaricity effect is also attributed to the appearance of the so-called mesothermal temperature maximum layer (MTML) in the winter period in the water column of Lake Baikal. The presence of MTML in Lake Baikal was discovered by G.Yu. Vereshchagin [5]: "in conditions of presence in the upper zone of reverse and in the lower zone of direct thermal stratification there should be the highest temperatures in the vertical profile, which at this time should be, approximately, equal to the temperatures of the maximal water density at a given depth; this intermediate zone we will call a zone of "mesothermal maximum"". Later, such mesothermal temperature maximum layer, which separates the upper, seasonally ventilated layer from the permanently stratified layer below and its effect on circulation in Great Bear Lake was investigated by Johnson [23].

It is known [8], that the cooling and mixing processes of the upper layer of the lake differ significantly when surface temperatures are above and below T_{md} ($\sim$4 °C). In early fall, while the lake has summer temperature stratification and its surface is warmer than T_{md}, the wind-induced shear turbulence is accompanied by convection due to gravitational instability (since the thermal expansion coefficient $\alpha > 0$, cooled water becomes denser than the water below and sinks). This obviously leads to accelerated deepening of the convective mixed layer. Then, gradually, surface temperature crosses 4 °C, and the active layer of the Lake Baikal becomes close to isothermal. Near this temperature, the thermal expansion coefficient becomes so small that its pressure dependence begins to play an essential role, and a mesothermal temperature maximum layer starts to form and deepen [19]. Thus, the MTML depth (at which the local temperature is equal to the temperature of maximum density at constant pressure) determines the transition between forced and free convection. Above this depth, the wind must work against buoyancy forces during cooling. As the lake cools further, the pressure dependence becomes less important, buoyancy flux increases, and the layer of actively wind-mixed water is restricted to progressively smaller depths [19]; by the time of ice formation, the final winter temperature profile is formed. Thus, the

resulting winter profile and the temperature and depth of the MTML should reflect the meteorological forcing in the preceding periods.

Vereshchagin G.Yu., in his study [5,24], hypothesized that the depth of the MTML depends on the intensity of wind mixing in the late autumn period before the lake freezes (November–January). Later [6,11], it was corroborated that the maximum temperature T_{mm} in the MTML layer is close to the temperature of the maximum density T_{md} at the depth of its occurrence. In turn, the depth of the mesothermal maximum $H_{T_{mm}}$ is the limit of development of free temperature convection in the following spring and summer and is also comparable to the lower boundary of the active layer in Lake Baikal (220–250 m) [6].

The aim of this study is to determine the spatial and temporal variability of the mesothermal temperature maximum layer in the winter period in Lake Baikal and its relationship with the meteorological forcing in the preceding summer and late autumn.

2. Materials and Methods

The western part of the southern basin of Lake Baikal, as the most covered by observations in the winter period, was chosen as the object of study in this work (Figure 1). The source materials were CTD soundings of the water column during the period of inverse stratification and year-round data on the vertical temperature distribution obtained from a mooring during the period from 2000 to 2022. ERA5-Land reanalysis data were used for meteorological forcing. For the analysis, the area covering the main circulation cell of the western part of the southern basin of Lake Baikal was chosen (according to Verbolov's map of mean Baikal currents [25]). The ice-on and ice-off dates were determined by visual observation by personnel from the shore at the neutrino telescope Baikal-GVD and near the Listvyanka settlement and additionally controlled by daily MODIS satellite imagery [26]. The ice-on dates were determined by the complete ice covering over the entire Southern Baikal (i.e., wind influence is completely excluded). The ice-off dates were determined as the beginning of ice breakup in Southern Baikal and a significant increase in wind forcing on the water column, respectively.
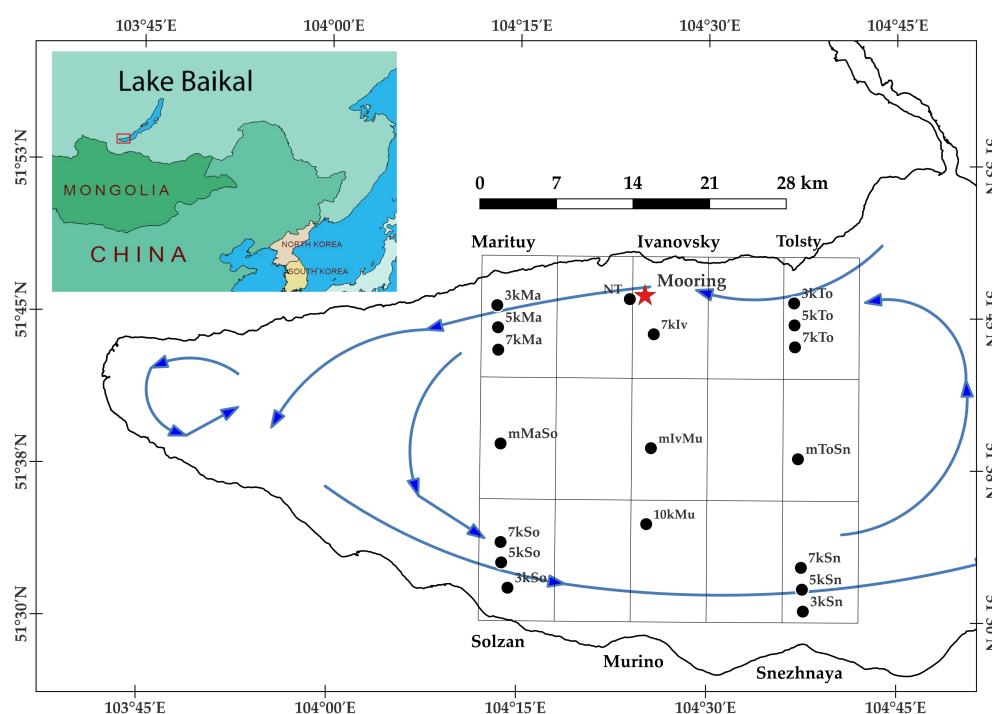
Figure 1. Location of study area (red rectangle in the inset) and scheme of measurement stations in Southern Baikal: dots—CTD stations, star—mooring, grid—area of ERA5-Land reanalysis data used for meteorological forcing. Blue arrows—mean currents pattern in study area.

2.1. CTD Measurements

The CTD data were obtained in February–April in the years 2000–2022 during winter field works from the ice cover and in May–June in the course of the first expeditions on research vessels after ice-off. CTD probing was carried out in Southern Baikal on transverse transects: Marituy settlement–Solzan River, Cape Ivanovsky–Murino settlement, and Cape Tolsty–Snezhnaya River (Figure 1). Temperature measurements (with 0.0003 °C resolution and ±0.002 °C absolute accuracy) were conducted with a Sea–Bird SBE–25 probe. The maximum temperature in MTML (T_{mm}), its depth ($H_{T_{mm}}$), and depth of the upper boundary of MTML which is equal the lower boundary of the thermocline (H_{up}) were determined on each temperature profile (See Section 3.2 for details).

To determine the spatial averaged T_{mm}, $H_{T_{mm}}$, and H_{up} for each winter, data were averaged over the February—early April period when winter spatial measurements from the ice were usually taken.

2.2. Mooring Data

Year-round temperature series obtained during 2000–2022 years at the full-depth mooring near the Baikal Neutrino Telescope (Baikal-GVD) were used in this research. The mooring (marked as a star in Figure 1) is located in the southern basin of Lake Baikal (104°30′ E, 51°45′ N) at a distance of 3.5 km from the shore, near Cape Ivanovsky.

At this point, regular long-term high-precision measurements of the temperature were started in March 1999, in cooperation with the Irkutsk State University (ISU), Joint Institute for Nuclear Research (JINR), Swiss Federal Institute of Environmental Science and Technology (EAWAG), and the Limnological Institute of the Siberian Branch of the Russian Academy of Science (LIN SB RAS) [27]. Historically, the mooring was equipped with a wide variety of temperature loggers: Vemco 12 bit minilog 64 K (resolution 0.015 °C, accuracy 0.1 °C); RBR TR-1000 (resolution 0.002 °C, accuracy 0.05 °C); TR-1050 (resolution 0.0001 °C, accuracy 0.002 °C); TR-1060 (resolution < 0.0005 °C, accuracy 0.002 °C); TDR-2050 (resolution 0.0001 °C, accuracy 0.002 °C); and more recently with RBRsolo T (resolution < 0.00005 °C, accuracy 0.002 °C).

Sensors were placed throughout the depth of the lake ranging from 4 m above the bottom to 11–43 m below the lake surface. Depths varied slightly from year to year, with the highest concentration of sensors in the active layer (down to 250 m) and near-bottom zone (see Figure 2). Additionally, about three to seven thermal sensors were installed in the MTML occurrence area in different years.

Thermistors were set up for regular in situ temperature measurements at intervals ranging from 15 s to 15 min. Every year in March, the station was retrieved for several days for maintenance to read data, replace batteries, and clean or replace failed loggers.
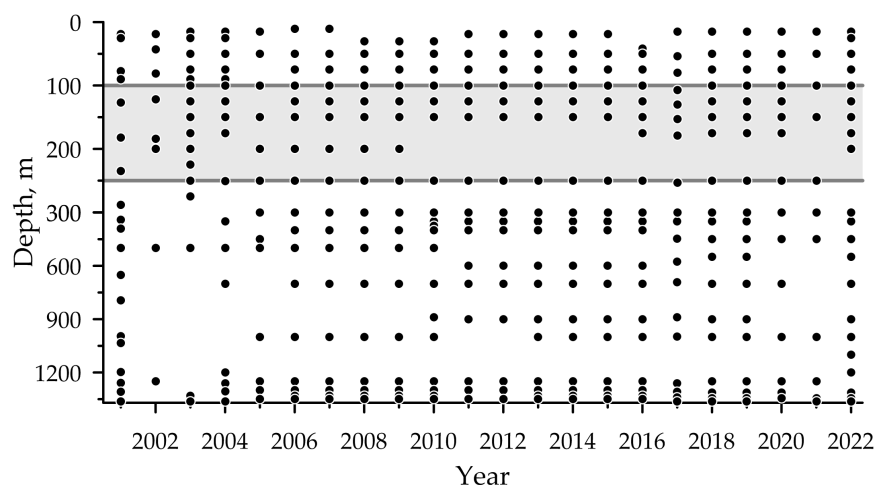
Figure 2. Vertical positioning of the temperature sensors at the mooring from 2000 to 2022. The gray zone is the area of the MTML layer. Note the different scales above and below 300 m.

Daily T_{mm} in MTML was defined as the maximum of the diurnal mean temperatures among sensors on the vertical profile. To determine the temporal average T_{mm} for each winter, daily T_{mm} data were averaged over a period of 20 to 90 days from ice formation. The first 20 days were excluded to reduce the influence of internal waves and currents generated by autumn winds, which gradually decrease by February [25,28]. According to measurements of the currents during the under-ice period in South Baikal, they lie on average in the range of 2–3 cm s^{-1} [29]. Taking into account that the ellipse length of the circulation cell (Figure 1) is approximately 120 km, its turnover time will be in the range of 46–70 days. Therefore, the averaging scale close to its maximum value was chosen.

Also, according to the daily mean of the upper temperature sensor on the mooring, the moment of its transition through the temperature of maximum density (~4 °C) was determined as the number of the days before 1 January. Using this result and the number of days after 1 January until ice-on, the fall cooling period (parameter $Days_{cool}$) was calculated for each year as the sum of these two intervals.

2.3. Meteorological Data and Wind Kinetic Energy Calculation

Observational data are the most reliable tool of any study, but in practice it often turns out that data are either missing or insufficient for the task at hand. In such cases, weather reanalysis data are used. The advantage is the completeness and homogeneity of the data provided as well as the coverage of areas difficult to access for ground-based observations. In our work, we needed to analyze wind activity over the lake water area. Since there are no permanent observations over the lake, we applied the well-known reanalysis of the European Centre for Medium-Range Weather Forecasts, in its most recent detailed release ERA5-Land [30], which aims to generalize the global meteorological monitoring network based on a four-dimensional variational assimilation system of retrospective data collected in the most complete base (with a grid step of 0.1 degree and a temporal resolution of 1 h).

Hourly data on wind speed (u_{10} and v_{10} components), air temperature T_{air}, dewpoint temperature T_r and surface pressure p were taken in the grid nodes shown in Figure 1 (the index "10" hereafter corresponds to the measurements or calculations at a standard height of 10 m). The values of wind kinetic energy flux from the atmosphere P_{10} were calculated on their basis. Then, obtained energy flux values and air temperatures were averaged over the grid area (Figure 1) for each day. Based on these data, for each year, mean wind kinetic energy and air temperature for summer (P_{summer} and T_{summer}) and late fall cooling period (P_{winter} and T_{winter}) were calculated. June–July was selected as the summer period, and 49 days before ice cover formation was selected as the late fall cooling period (which is the average number of days for all years considered).

According to [31], energy flux from the atmosphere at a height of 10 m above the water, P_{10}, is given by:

$$P_{10} = \tau_0 W_{10} = \rho_{air} C_{10} W_{10}^3 \tag{1}$$

where τ_0 is wind stress, ρ_{air} is air density, C_{10} is drag (wind stress) coefficient, and W_{10} is the wind speed modulus determined from u_{10} and v_{10} components. Parametrization from the [32] was used to calculate the drag coefficient:

$$C_{10} = C_{DN} = 1.7 \times 10^{-3}[1 + exp(-1.1W_{10})] \tag{2}$$

Following the recommendations of the "International Committee of Weights and Measures" (ICMW) in accordance with [33], the following equation is used to calculate the density of moist air:

$$\rho_{air} = \frac{pM_{air}}{ZRT}\left[1 - \chi_V\left(1 - \frac{M_V}{M_{air}}\right)\right] \tag{3}$$

where p—is the air pressure, $M_{air} = 28.96546 \times 10^3$ kg mol^{-1} is the molar mass of dry air, Z is the compressibility factor, R is the molar gas constant, T is the thermodynamic temperature according to IPTS-90, χ_V is the molar mass of water vapor, and M_V is the molar mass of water. Algorithms for determining Z and χ_V are also given in [33].

2.4. Statistical Methods

All analyzed parameters characterizing the years under study were divided into two groups: the dependent variables T_{mm}, $H_{T_{mm}}$, $Days_{cool}$, and H_{up} and the responsible factors P_{summer}, P_{winter}, T_{summer}, and T_{winter}. The assessment of the reliability of the relationship between dependent variables and responsible factors was carried out using the Mantel test [34] based on matrices of pairwise Euclidean distances and Pearson's correlation coefficient. The reliability of the value of the correlation coefficient is determined by a permutation test (5000 permutations), the relationship was considered significant at $p \leq 0.05$. The analysis was carried out in the "vegan" [35] package for the R programming language. Visualization of multivariate data for years characterized by dependent variables and responsible factors was carried out using the principal component analysis (PCA) method. Before using PCA to level the influence of dimensionality, the data for each variable were normalized by ranging from 0 to 1. The analysis included responsible factors that showed a significant relationship with dependent variables according to the results of the Mantel test. The analysis was carried out using the packages "vegan" [35] and "factoextra" [36] for the R programming language.

3. Results

3.1. Phenology of Hydrological Events

Important moments in the annual course of lake water temperature are the transitions of its surface temperature through the temperature of maximum water density (T_{md}). In the fall, this involves a transition from summer temperature stratification to winter stratification and vice versa in the spring. Also significant are the dates of the lake ice-on and ice-off as well as the duration of the fall cooling period ($Days_{cool}$—the number of days from the date of the transition of surface water temperature through 4 °C to the ice-on).

Analysis of the phenology of hydrological phenomena (Figure 3) showed that both the dates of temperature transition through 4 °C and the dates of ice-on over the observation period had positive trends (9.2 and 3.3 days per 10 years respectively). On the contrary, the duration of autumn cooling and the date of ice-off decreased at a rate of 5.7 and 8.7 days per 10 years, respectively. Validity assessment showed that changes in the timing of water temperature transition through 4 °C (r = 0.46, p = 0.02) and ice-off dates (r = 0.59, p = 0.002) have significant trends. The changes in the duration of the fall cooling period and the date of the ice breakup beginning are insignificant (r = 0.27, p = 0.21 and r = 0.23, p = 0.28, respectively).
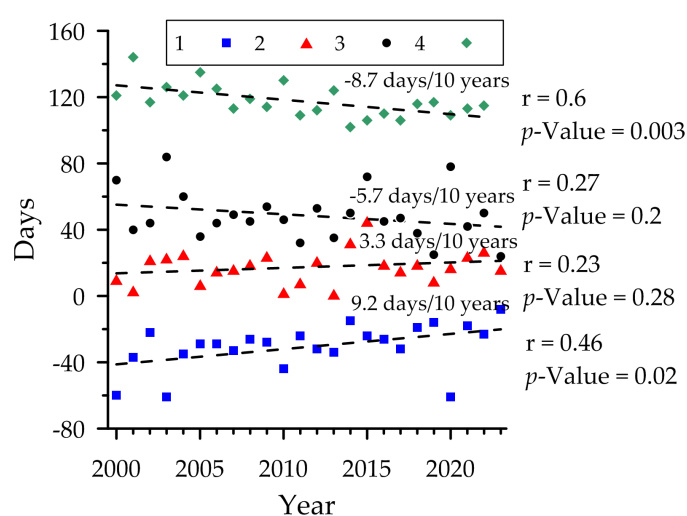
Figure 3. Number of days relative to 1 January (taken as zero) and duration of hydrological events during the observation period, and their trends: 1—number of the day when temperature at the upper sensor of the mooring crossed 4 degrees, 2—number of the day when ice-on occurs, 3—duration of the fall cooling period, 4—number of the day when ice-off occurred.

3.2. Comparison of Mooring and CTD Data

Preliminary analysis of the CTD data showed a large inter-annual and spatial variability of the vertical temperature profiles (see several examples in Figure 4).
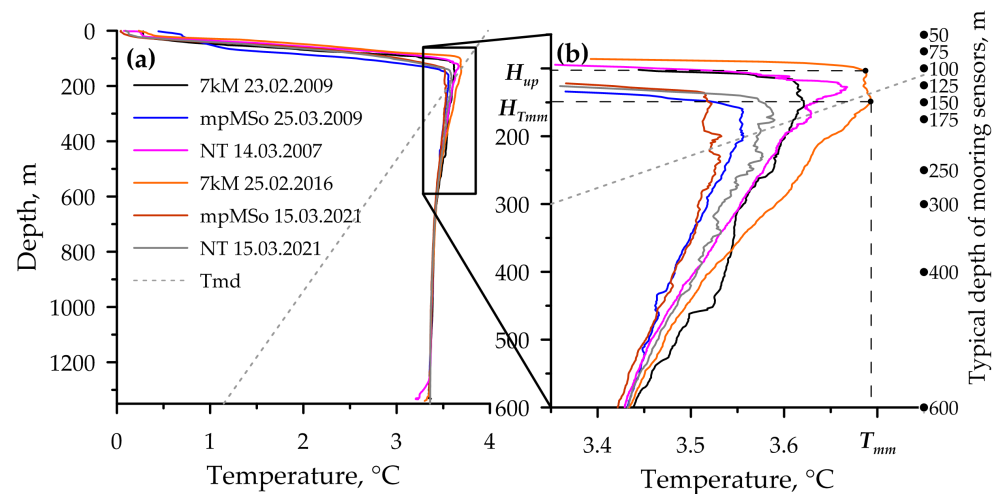
Figure 4. (**a**) Typical vertical distribution of winter temperature in Southern Baikal in comparison with the dependence of temperature of maximum density (T_{md}) on pressure. (**b**) The same in magnified scale. The 2016 profile shows how T_{mm}, $H_{T_{mm}}$ and H_{up} were determined. The typical location of the mooring sensors given on the right shows that they cover the area of interest (MTML).

Below the ice cover, water temperature in Lake Baikal exhibits a distinct thermal stratification. Directly under the ice, the temperature in the first meter experiences a sharp jump from 0 °C to 0.05–0.5 °C. Then, there is a relatively mixed layer of radiatively driven convection, whose thickness gradually increases in spring with the raising of incoming solar radiation (from meters to tens meters). Afterwards water temperature rises uniformly and quickly (thermocline layer), reaching its maximum value T_{mm} at depth $H_{T_{mm}}$ in MTML. The lower boundary of the thermocline is the upper boundary H_{up} of the mesothermal maximum layer, whose temperature lies in the range of 3.5–3.7 °C (Figure 4b). The MTML layer can be as small as 10–20 m or reach thicknesses of more than 150 m. Below the MTML, the temperature drops gently to 3.36 °C in South Baikal. Deeper than 700 m, interannual temperature differences usually do not exceed 0.02 °C, and only in the near-bottom 100 m region, temperature deviations up to tenths of a degrees are possible, indicating the processes of deep water renewal.

Despite the different depth of MTML occurrence, the temperature gradient in the main part of the thermocline located above is approximately constant and equal to 40 ± 5 m°C m^{-1}. Below the MTML in the deep region, the temperature gradient is divided into two characteristic sections: up to a depth of 700 m the gradient is two orders of magnitude smaller and is about 0.4 ± 0.1 m°C m^{-1}, and then the temperature profile experiences a bend and further to the bottom the gradient at all stations is approximately the same and is equal to 0.09 ± 0.01 m°C m^{-1}.

Figure 5 shows the maximum temperature in the MTML found during the period of its existence (approximately from November to June of each year) using different input data (daily average from mooring data and momentary from CTD).

It can be seen that the T_{mm} variations during individual winters by water area (CTD data) and by time (mooring data) are approximately of the same order. According to CTD data, T_{mm} ranged within 3.527–3.747 °C (mean 3.638 °C), its depth $H_{T_{mm}}$ varied from 104 to 230 m (mean 149 m), and the upper boundary of the MTML H_{up} ranged within 94–184 m (mean 132 m). According to the data in Figure 5, the average winter T_{mm} values were calculated. Figure 6a shows a comparison of spatial and temporal averaging of T_{mm}. Despite the high correlation coefficient between the various averages, the difference between them in some years can reach 0.05 °C. Therefore, it was decided to take the average

of the combined CTD and mooring data as the mean winter temperature (the result of the combined average is shown by crosses in Figure 5).
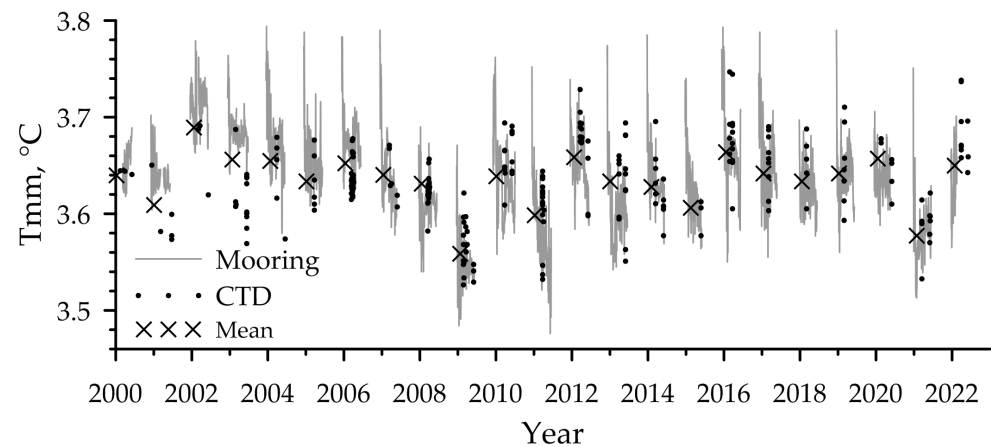
Figure 5. Maximum temperatures in MTML for the whole period of measurements. Lines—daily averaged mooring data, dots—CTD data. Crosses—mean winter T_{mm} values determined from a combination of CTD and mooring data.
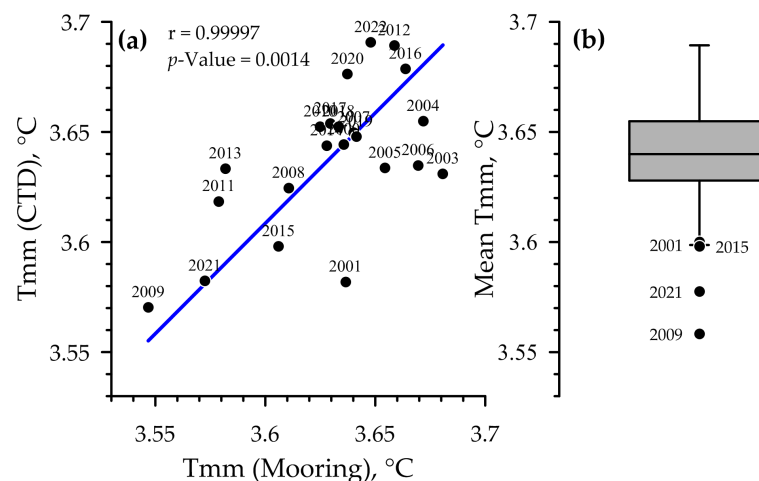
Figure 6. In situ data analysis: (**a**) comparison of mean winter T_{mm} obtained by spatial (CTD) and temporal (mooring) averaging. (**b**) box-plot for mean winter T_{mm} with outlier years.

The relationship between mean winter T_{mm} obtained by spatial (CTD) and temporal (mooring) averaging is shown in detail in Figure 6a, and the results of box-plot analysis of the combined mean T_{mm} in Figure 6b. According to the box-plot analysis, outlier years were identified. As a consequence, 2001, 2009, 2015, and 2021 were excluded from the comparative analysis of MTML characteristics with meteorological forcing. Since the T_{mm} values in these years differ sharply from the values in the rest of the measurement period, they require an individual special consideration.

An analysis of the mean winter depths of the upper boundary of MTML H_{up} and the depths of maximum temperature $H_{T_{mm}}$ as a function of T_{mm} (Figure 7) indicates that decrease in maximal temperature in MTML is accompanied by deepening of its depth and upper boundary of MTML. Thus, this behavior is consistent with the dependence of temperature of maximum density T_{md} on depth.
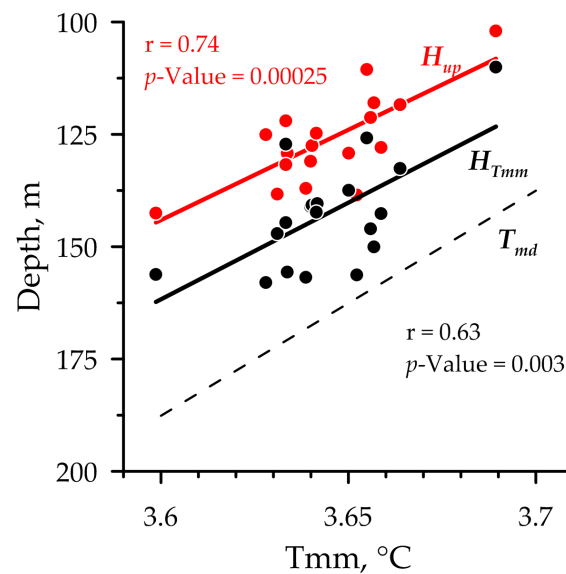
Figure 7. Dependence of the depth of the upper boundary of MTML (H_{up}, red circles and trend line), and the depth of maximum temperature ($H_{T_{mm}}$, black circles and trend line) on mean winter T_{mm} in comparison with the dependence of temperature of maximum density (T_{md}, dotted line) on pressure.

3.3. Variations in T_{mm} during Winter

Analysis of the variability of T_{mm} in the MTML during winter for different years reveals four different types of its mean trends behavior; examples are given in Figure 8.
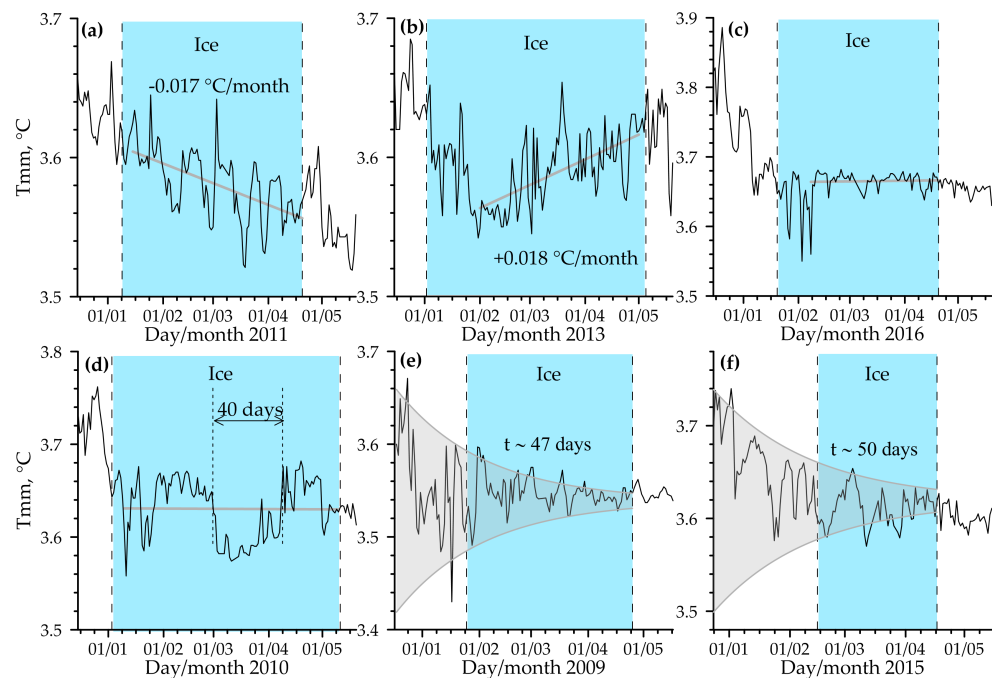
Figure 8. Examples of variations in T_{mm} temperature during winter in different years (**a**–**f**); blue areas indicate ice-covered periods.

The MTML layer begins to form after the surface temperature crosses 4 °C. During the period of fall cooling, it gradually deepens, accompanied by a decrease in T_{mm} temperature, which is clearly seen for all years (Figures 5 and 8). In 2007, 2011, 2014, and 2021, the decreasing trend of T_{mm} continued throughout the winter (example in Figure 8a). The temperature decreased at a rate of 0.01–0.02 °C/month. In contrast, in 2008, 2013, 2017, and 2020, there was a gradual increase in T_{mm} during the under-ice period at a rate of

0.01–0.018 °C/month (example in Figure 8b). In other years, no significant trends (more than 0.01 °C/month) of T_{mm} during winter were recorded, but other specific features of its behavior were noted. For example, in 2010 (Figure 8d), a sharp drop in water temperature occurred on 27 February. The subsequent time of water temperature recovery to its maximum values was about 40 days. In 2009 and 2015, the temperature trends were close to zero, but attenuated fluctuations of T_{mm} were observed (example in Figure 8e,f). The time constant of the damped oscillations was about 47–50 days.

### 3.4. Dependence of MTML Parameters on Meteorological Forcing

Table A1 summarizes all input data for the investigation of meteorological forcing on MTML parameters, including those years that were discarded in the box-plot analysis. The supply of mechanical energy by wind showed slight seasonal variations and was minimal in summer (mean P_{summer} = 74 ± 12 mW m^{-2} with corresponding mean wind speed W_{summer} = 2.61 ± 0.11 m s^{-1}) and maximal in late fall (mean P_{winter} = 91 ± 22 mW m^{-2} and corresponding W_{winter} = 2.66 ± 0.22 m s^{-1}). The results of the Mantel test (Table 1) show that dependent variable T_{mm} was significantly related to P_{summer} and P_{winter}, the dependent variable $H_{T_{mm}}$ was reliably correlated with P_{summer}, the dependent variable $Days_{cool}$ was correlated with T_{winter}, and the dependent variable H_{up} was strongly associated with P_{summer}. The responsible factor T_{summer} did not reliably influence any of the dependent variables. In terms of intensity of influence on dependent variables, based on the values of the Pearson correlation coefficient, P_{summer} takes the leading role, followed by P_{winter}, and the last is T_{winter} (Table 1).

Table 1. Mantel test result for analyzing the relationship between dependent variables and responsible factors.

Dependent Variable	Explanatory Parameter	r	*p*-Value
T_{mm}	P_{summer}	**0.364 ***	**0.036**
	P_{winter}	**0.354**	**0.021**
	T_{summer}	0.012	0.460
	T_{winter}	0.231	0.121
$H_{T_{mm}}$	P_{summer}	**0.381**	**0.039**
	P_{winter}	0.088	0.196
	T_{summer}	−0.031	0.523
	T_{winter}	−0.129	0.792
$Days_{cool}$	P_{summer}	-0.050	0.591
	P_{winter}	−0.134	0.829
	T_{summer}	−0.031	0.578
	T_{winter}	**0.259**	**0.044**
H_{up}	P_{summer}	**0.322**	**0.035**
	P_{winter}	0.103	0.182
	T_{summer}	−0.004	0.479
	T_{winter}	−0.033	0.517

Notes: * bold type indicates responsible factors that significantly affect dependent variables ($p \leq 0.05$).

During principal component analysis, T_{summer} responsible factor was excluded from the data set, which did not show a reliable relationship with any dependent variables (see Table 1). PCA biplot analysis (Figure 9) shows that dependent variables and responsible factors form two groups according to gradient vectors. The first group includes P_{summer}, T_{mm}, H_{up}, and $H_{T_{mm}}$. In this group, an increase in P_{summer} leads to an increase in T_{mm} and a decrease in H_{up} and $H_{T_{mm}}$. The second group includes P_{winter}, T_{winter}, and $Days_{cool}$. In this group, an increase in P_{winter} entails a decrease in T_{winter} and a shortening of $Days_{cool}$.
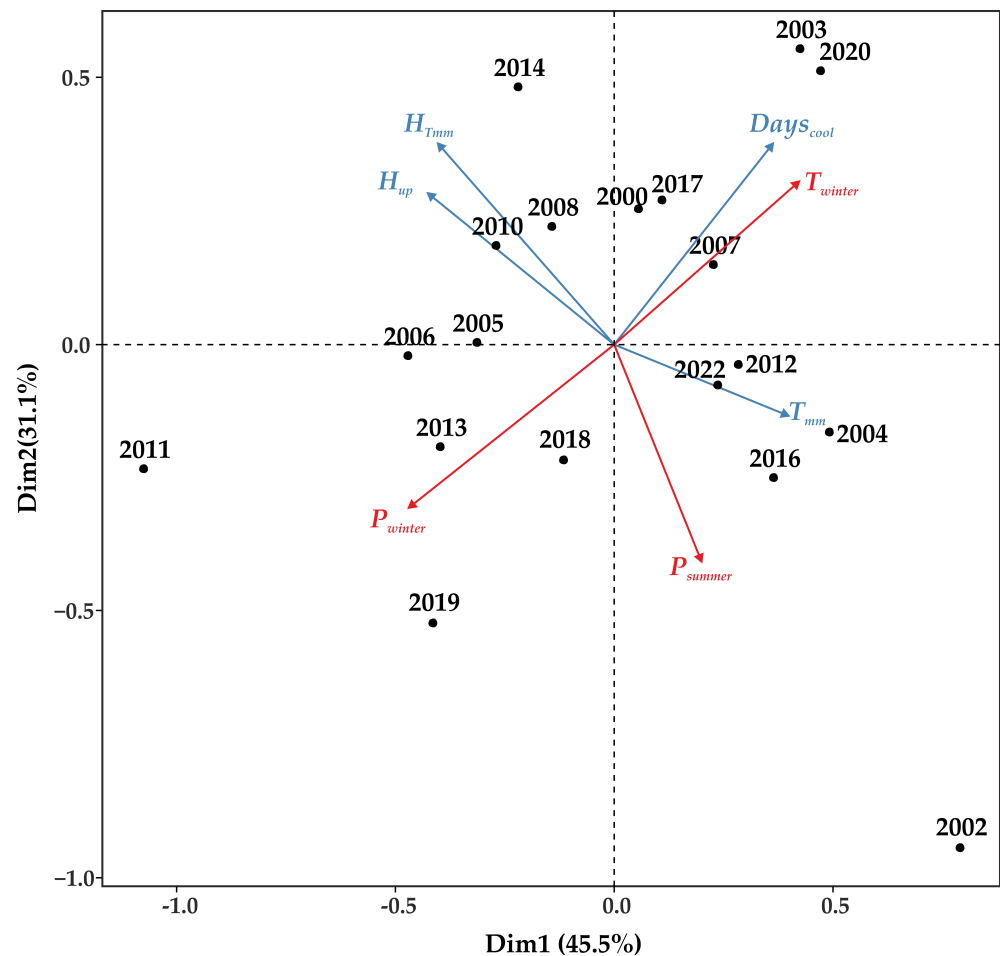
Figure 9. Result of principal component analysis based on dependent variable data—T_{mm}, $H_{T_{mm}}$, $Days_{cool}$, and H_{up} and responsible factors P_{summer}, P_{winter}, and T_{winter} by years. The red arrows show the gradient vectors of the responsible factors. The blue arrows show the gradient vectors of the dependent variables.

Regarding the analyzed data, all years can be divided into two groups. The first group includes the years 2002, 2004, 2007, 2012, 2016, 2018, 2019, and 2022. These years are characterized by high values of P_{summer} and T_{mm} and low values of H_{up} and $H_{T_{mm}}$. The second group includes 2000, 2003, 2005, 2006, 2008, 2010, 2011, 2013 2014, 2017, and 2020. This group is characterized by low values of P_{summer} and T_{mm} and high values of H_{up} and $H_{T_{mm}}$.

To analyze the dependence of MTML parameters on wind forcing in more detail, we investigated the dependence of T_{mm} on cumulative wind energy flux during summer and late fall periods (Figure 10), as well as the impact of cumulative wind energy flux on $H_{T_{mm}}$ and H_{up} depths (Figure 11) for all years considered.

A positive relationship between T_{mm} and cumulative wind energy flux during summer and a negative one in the period of late-autumn cooling is well traced. Both dependencies can be considered reliable ($p < 0.05$), and it can also be concluded that the relationship with summer winds is slightly higher than with winds in late fall (Figure 10).

In contrast to T_{mm}, the dependencies of the depth of the MTML upper boundary and the depth of the temperature maximum on cumulative wind energy fluxes are weaker (Figure 11). Only the dependencies of $H_{T_{mm}}$ on P_{summer} and H_{up} on P_{winter} can be considered more-or-less reliable. One can observe a deepening of H_{up} and $H_{T_{mm}}$ depths with strengthening of late fall winds, and their shallowing with the intensification of summer winds.
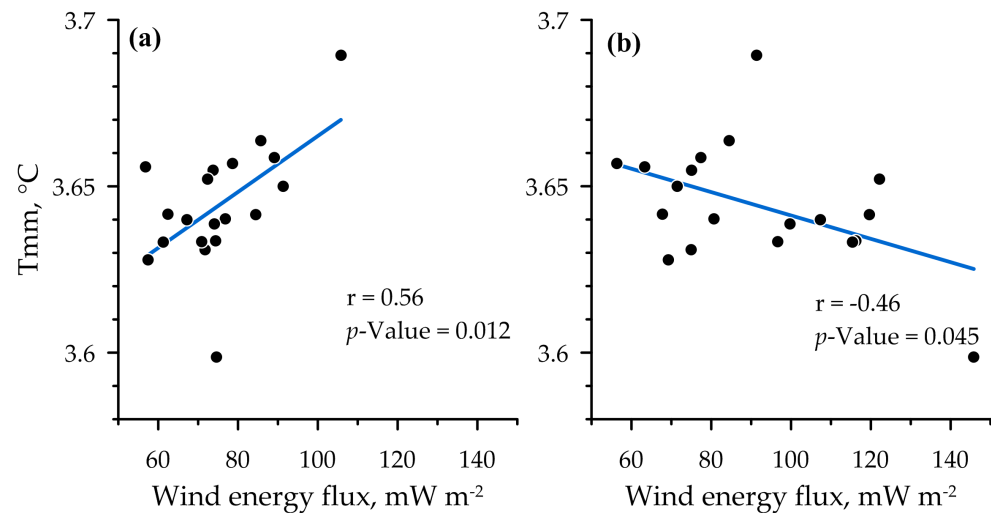
Figure 10. Comparison of mean winter T_{mm} on cumulative wind energy fluxes during (**a**) summer and (**b**) late-autumn periods.
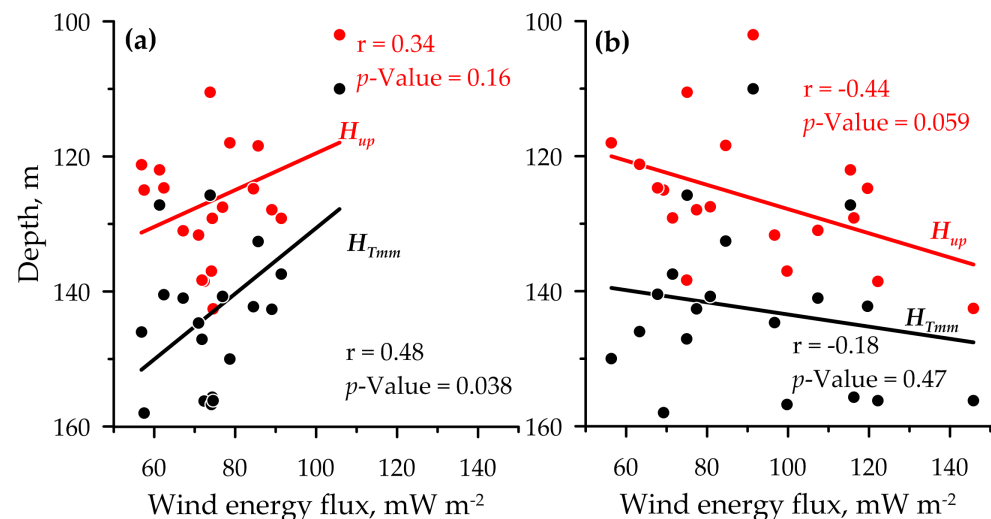
Figure 11. Comparison of the depth of the upper boundary of MTML (H_{up}, red circles and trend lines) and the depth of maximum temperature ($H_{T_{mm}}$, black circles and trend lines) on wind energy during (**a**) summer and (**b**) late autumn periods for all years of measurements.

4. Discussion

Long-term spatial and temporal variability of the main parameters of the mesothermal temperature maximum layer in Lake Baikal was investigated on the basis of hydrophysical data from CTD soundings and the mooring station. Variations in T_{mm}, $H_{T_{mm}}$, and H_{up} were considered in the context of meteorological forcing and phenology of hydrological events. Although the 22 year period cannot be considered long enough to talk about climatic changes on a global scale, we can say with certainty that there were noticeable time shifts in some of the analyzed hydrological events during this period (Figure 3). The multidirectional trends of ice cover formation and breakup indicate that the total duration (and hence thickness) of the ice cover is gradually decreasing.

The noted tendencies of changes in the phenology of the considered hydrological events (Figure 3) are in agreement with the previously noted trends in longer series of observations [37–47]. Also, Shimaraev et al. [48], revealed an increase in water temperature in March–July in the upper 300-meter layer in South Baikal in 1972–1992, and then (1995–2007) its decrease. Later [47], studies of the spatial features of the surface layer water temperature response in 1970–2016 showed a decrease in the positive trend of water temperature in Southern Baikal, especially after 1995. In deeper layers in South Baikal, there has been a

decrease in water temperature since 1995 [48]. The persistence of these trends is confirmed by the results of studying the changes in the heat content Q in the water column of Southern Baikal. According to the mooring data, the analysis of changes in Q values [49] revealed a significant positive trend in the upper 100-meter layer in May and its absence in other months. Deeper, the trends of Q values were negative.

In the 21st century, the trend of increasing the open water period and, consequently, decreasing the ice-over period due to the rising water temperature in winter-spring and summer periods continues. Shortening the duration of ice cover can have several potential dangers and implications for the ecosystem of the lake because ice cover plays a crucial role in its ecology. It provides a physical barrier that regulates the exchange of gasses between the water and the atmosphere, affects light penetration, and influences nutrient cycling. Shortening the ice cover duration can disrupt these processes, leading to changes in water temperature, reduced dissolved oxygen levels, altered nutrient dynamics, and shifts in the timing of biological events (phytoplankton bloom and others). These ecological changes can impact the entire food web, from primary producers to higher trophic levels. Also, decreased ice cover can contribute to a positive climate change feedback loop, as reduced reflection of sunlight (albedo) from the lake surface leads to increased absorption of solar energy, further warming the water. This feedback, as well as changes in the intensity of vertical mixing processes [17], can amplify regional or local temperature changes and contribute to the overall warming trend.

In spite of essential trends in the dates of occurrence of hydrological events (Figure 3), no noticeable trends were registered for the mean wind speeds during the summer (r = 0.19) and late fall (r = 0.02) periods in 2000–2022 (Table A1). It is noteworthy that wind speeds during the period under study were noticeably lower than in the middle of the 20th century [10]. Comparison of mean wind speeds for individual months in 1959–1968 and in 2000–2022 revealed their decrease in June–August by 0.8–1.1 m s^{-1}, in September–November by 1.1–2.0 m s^{-1}, in December by 2.4 m s^{-1} and in January by 1.4 m s^{-1}. Such changes are registered in most territory of Russia [50] and are probably caused by rapid warming in the Arctic and decrease in the poleward temperature gradient which could influence mid-latitude circulation and intensity of winds [51]. Based on this, we can assume that in the present time the MTML on average forms shallower and has higher temperatures compared to the 20th century. Our assumption is supported by the results of previous studies [5,52], which report the formation of MTML within 200–400 m with maximum temperatures of 3.4–3.9 °C. Later, when measurements on standard sections began, Shimaraev [53] gave an estimate of MTML occurrence within 150–300 m with temperatures in the range of 3.5–3.8 °C. Even if we take into account that the accuracy of measurements in those years was within ±0.02–0.1 °C, the results of previous studies [5,52,53] confirm our assumptions.

The lack of trends in mean wind speeds was also accompanied by a no noticeable trends in MTML temperatures T_{mm}, and depths H_{up} and $H_{T_{mm}}$ over 2000–2022. However. there was significant variability in these characteristics from year to year (Figure 5). Our study showed that the main influencing factors are the intensity of winds in summer and late-autumn periods. At the same time, average summer and late-fall temperatures, although varying from year to year, do not have a considerable impact (Tables 1 and A1). Increased wind activity in summer leads to the formation of MTML closer to the surface (small values of H_{up} and $H_{T_{mm}}$) with high values of T_{mm}. At decreased wind activity, the opposite situation is observed: the H_{up} and $H_{T_{mm}}$) deepen, and T_{mm} values decrease (Figures 10 and 11). This is explained by the fact that at higher wind speeds during the period of summer stratification, due to wind-wave mixing, a thicker epilimnion layer is formed with small vertical temperature gradients in the thermocline. Accordingly, water warming by the end of the summer stratification period is observed to deeper depths (several tens of meters). Then, in autumn, since the temperature at the surface is lower, the transition to reverse stratification occurs earlier and the heat in deeper layers is retained in the water column rather than escaping to the atmosphere. At low wind speeds during the summer stratification, a small epilimnion with higher temperatures and large

vertical gradients in the thermocline is formed. When the fall cooling begins, heat from the epilimnion escapes more rapidly to the atmosphere due to the larger temperature difference between air and water surface and intensive wind mixing. Thus, MTML is formed more blurred with less T_{mm} temperature. It is worth noting that the ratio between the effect of air–water temperature differences and the strength and duration of wind forcing is important here.

Increased wind activity in late fall (when the surface temperature drops below 4 °C) leads to the reverse processes. At this time, stable temperature stratification begins to form in the upper layer of the lake, as water becomes less dense with further cooling and, accordingly, tends to the surface. Since water above the T_{md} line (Figure 4b) is stably stratified, turbulent mixing can only be maintained by mechanical energy input due to the wind. Thus, without wind influence on the lake during this period, the temperature profile with very shallow MTML and its temperature close to 4 degrees should be formed in winter [54]. And, as the wind energy input (P_{winter}) intensifies, MTML, accordingly, deepens (Figure 11b) and its temperature decreases (Figure 10b).

Thus, the dependence of MTML characteristics on both the intensity of summer and late-fall winds was revealed, and at the same time, they themselves are practically independent of each other (vectors P_{summer} and P_{winter} on the PCA diagram are located at nearly a right angle (Figure 9). Consequently, their influence is complex and, therefore, separately they show not very high correlation coefficients with maximum temperature and depth of MTML.

The analysis of the mean winter depths of the upper boundary of the MTML and the depths of the maximum temperature as a function of T_{mm} (Figure 7) shows that the decrease in the maximum temperature in the MTML is accompanied by a deepening of its depth $H_{T_{mm}}$ and the upper boundary of the MTML H_{up}. Expectedly, this behavior is consistent with the dependence of the maximum density temperature T_{md} on depth. In addition, these values are always smaller than the depth of T_{md}. However, considering specific cases of instantaneous vertical temperature distribution (Figure 4) we can observe that the depths of T_{mm} are larger than the depth of T_{md}. This is due to the occurrence of thermobaric instability conditions and the forced sinking of surface water masses with temperatures higher than T_{md} deeper than the T_{md} profile. Analysis of the variability of T_{mm} in the MTML during winter in different years reveals various types of behavior of its mean trends (Figure 8). Despite a rather wide range of trends in some years (from -0.02 to $+0.018$ °C/month), the most common situation is a negligibly small MTML temperature trend.

In 2007, 2011, 2014, and 2021, the decreasing T_{mm} trends during the winter were observed (example in Figure 8a). Late ice-on dates prevailed in these years (18 January, 2 February, and 25 January for 2007, 2014, and 2021, respectively), except for 2011, when ice-on was early (10 January). This was primarily due to decreased wind activity during the fall cooling period: P_{winter} values were in the range of 69–95 mW m^{-2} for these three years, while in 2011 it was 146 mW m^{-2} which was 1.6 times higher than its multiyear average (91 mW m^{-2}). In addition, according to the data of [47] in 2011, out of these four years, the highest surface water temperature (8.958 °C) averaged over May–September (hereinafter data for the surface water temperature in Listvyanka settlement are given), and the maximum heat content (2728.8 MJ m^{-2}) in the upper 100-meter water layer Q_{100} for the period of heat accumulation (May–September) were observed [49].

In 2008, 2013, 2017, and 2020 (example in Figure 8b), in contrast, there was a gradual increase in T_{mm} values during winter. In 2013 and 2020, the ice-on was early (3 January and 12 January, respectively), while in 2008 and 2017 it was slightly later (21 January and 20 January, respectively). Wind energy input P_{winter} during the fall cooling period was lowered in three years (56–75 mW m^{-2}) except 2013 (97 mW m^{-2}). It is worth noting that in 2013, the mean May–September water surface temperature was the lowest (6.311 °C), while the Q_{100} was one of the largest (2313.8 MJ m^{-2}) among these years [47,49].

In other years, no significant trends in T_{mm} temperature were observed during the winter (example in Figure 8c). The ice formation was mostly late and occurred mainly in

the third decade of January. The exceptions are years with early (5 and 4 January in 2001 and 2010) and intermediate ice-on dates (12 and 9 January in 2000 and 2005). In 2015, the latest ice formation date (15 February) for the entire observation period (1869–2022) was observed. In terms of Q_{100}, 2003 (with a minimum value of 1721.1 MJ m^{-2}) and 2012 (with a maximum, 3326.5 MJ m^{-2}) are distinguished. The mean May–September water surface temperature was also lowest in 2003 (6.08 °C), but highest in 2016 (9.61 °C). The wind energy P_{winter} varied widely (63–122 mW m^{-2}).

The years 2009 and 2015 should be especially noted, as during those winters damped T_{mm} oscillations were observed (Figure 8e,f). The calculated time constant of oscillations (47 and 50 days, respectively) is comparable with the damping time scales of 38 ± 2 and 42 ± 3 days determined from the decay of current kinetic energy and dissipation, respectively, in the under-ice period on Lake Baikal [55]. The dates of the ice formation onset were observed late (26 January in 2009 and 15 February in 2015). Wind energy values during the fall cooling period were lower than the mean annual value in 2015 (71 mW m^{-2}) and slightly higher in 2009 (101 mW m^{-2}). The Q_{100} and May–September mean water surface temperature values were similar for both years (2701.7 MJ m^{-2} and 8.774 °C in 2009) and (2788.7 MJ m^{-2} and 9.01 °C in 2015).

Also interesting was 2010 (Figure 8d), in which a sharp drop in T_{mm} temperature occurred in the middle of winter. The time of water temperature recovery was about 40 days. It may be connected with deeper mixing near the southern shore with gradual transfer by the circulation cell to the mooring area. The recovery time is comparable to a half-turn of the cell at under-ice currents velocity of about 2 cm/s. Analysis of water temperatures on mooring during the fall period showed that they were also characterized by abrupt, jump-like changes, especially noticeable in the MTML. Ice breakup this year was early (January 4), and wind activity during the late fall period was close to the multiyear average (100 mW m^{-2}). Heat storage values Q_{100} as well as in the 100–300 m layer Q_{300} were above the multiyear averages (2486.2 and 3216.0 MJ m^{-2}, respectively) [49]. At the same time, the water surface temperature for May–September was minimal among 2000–2022 (6.08 °C) [47].

5. Conclusions

For the first time, the long-term spatial and temporal variability of the mesothermal temperature maximum layer in Lake Baikal was investigated on the basis of CTD and mooring data. Changes in various MTML parameters (maximal temperature, its depth, and the depth of the upper boundary of the MTML) were examined as a function of meteorological forcing in summer and late autumn. In spite of the essential trends over the study period in the dates of occurrence of hydrological events, no noticeable trends were registered for the maximum MTML temperature, its depth, and the depth of the upper boundary of the MTML.

Having analyzed the obtained data, we can summarize the following properties of mesothermal temperature maximum layer:

- Water temperature in MTML and temperature of maximum density are fairly close. There is inverse temperature stratification above and direct temperature below MTML. Therefore, MTML is the boundary between inverse and direct stratification, and its depth of occurrence determines the thickness of the surface layer of water with inverse temperature stratification;
- Water temperature profiles in the MTML have high spatial and temporal variability, which indicates the processes of intense vertical turbulent mixing and internal wave motions. This is also in accordance with the higher vertical diffusivity values at depths of 200–300 m relative to deeper layers reported in [55];
- In the MTML, vertical stability is minimal and the thermodynamic characteristics of water have a number of unique properties: water temperature is equal to maximum density temperature, and hence, the thermal expansion coefficient of water is close to zero;

- Depending on the influence of meteorological and hydrological conditions on MTML formation, four types of maximal temperature in MTML behavior during ice season were identified;
- It is shown that MTML formation is affected not only by wind conditions in the late fall (as previously assumed) but also in the summer period. At increased wind activity in summer, larger maximal temperatures in the MTML and smaller depths are observed. At decreased wind activity, the opposite behavior is noted.

In this paper, only a preliminary analysis of the obtained data has been carried out. But even then, it has already revealed certain tendencies. The work will be continued, and it is planned to analyze data on currents and other factors. More sophisticated approaches, including mathematical modeling, will be used.

Author Contributions: Conceptualization, I.A. and N.G.; data curation, I.A., E.T., R.G. and I.P.; Formal analysis, S.L.; funding acquisition, I.A. and S.L.; investigation, I.A.; methodology, I.A. and Y.B.; project administration, I.A.; software, R.G. and I.P.; supervision, N.G.; validation, I.A.; visualization, I.A., R.G. and Y.B.; writing—original draft, I.A.; writing—review and editing, I.A., E.T. and N.G. All authors have read and agreed to the published version of the manuscript.

Data Availability Statement: Data are available from the authors by request.

Conflicts of Interest: The authors declare no conflicts of interest.

Abbreviations

The following abbreviations are used in this manuscript:

MTML	Mesothermal Temperature Maximum Layer
T_{mm}	Maximal temperature in the MTML
T_{md}	Temperature of the maximum density of water
$H_{T_{mm}}$	Depth of the maximal temperature in the MTML
H_{up}	Depth of the upper boundary of MTML (or lower boundary of the thermocline)
$Days_{cool}$	Period of the fall cooling (Number of days passed from the moment of water surface temperature crosses T_{md} until the freezing of the lake)
u_{10}	Eastward component of wind speed at a height of 10 m above the surface of the Earth
v_{10}	Northward component of wind speed at a height of 10 m above the surface of the Earth
P_{10}	Wind kinetic energy flux from the atmosphere
C_{10}	Drag (wind stress) coefficient for the wind at a height of 10 m
W_{10}	Wind speed modulus at a height of 10 m above the surface of the Earth
P_{summer}	Mean wind kinetic energy flux for summer period
T_{summer}	Mean air temperature for summer period
W_{summer}	Mean wind speed modulus for summer period
P_{winter}	Mean wind kinetic energy flux for late fall cooling period
T_{winter}	Mean air temperature for late fall cooling period
W_{winter}	Mean wind speed modulus for late fall cooling period

Appendix A

Table A1. Results of calculated mean MTML parameters and meteorological forcing characteristics.

Year	T_{mm}°C	$H_{T_{mm}}$m	H_{up}m	$Days_{cool}$	W_{summer} m s^{-1}	P_{summer} mW m^{-2}	W_{winter} m s^{-1}	P_{winter} mW m^{-2}	T_{summer}°C	T_{winter}°C
2000	3.64	141	131	70	2.5	67	2.8	107	14.01	−8.43
2001	3.609	197	117	40	2.6	69	2.5	81	15.24	−12.89
2002	3.689	110	102	44	2.7	106	2.6	91	15.19	−10.8
2003	3.656	146	121	84	2.4	57	2.4	63	15.84	−8.93
2004	3.655	126	111	60	2.6	74	2.6	75	14.52	−10.52
2005	3.634	156	129	36	2.6	74	2.8	116	14.41	−9.03
2006	3.652	156	139	44	2.6	72	3.1	122	14.59	−12.53
2007	3.64	141	128	49	2.7	77	2.5	81	13.87	−6.49
2008	3.631	147	138	45	2.6	72	2.5	75	15.79	−10.12
2009	3.559	166	153	54	2.7	82	2.6	101	14.71	−11.61
2010	3.639	157	137	46	2.6	74	2.8	100	13.96	−9.75
2011	3.599	156	143	32	2.7	75	3.2	146	13.99	−16.15
2012	3.659	143	127	53	2.7	89	2.6	77	14.61	−8.93
2013	3.633	145	130	35	2.6	71	2.8	97	14.51	−14.73
2014	3.628	158	135	50	2.5	57	2.5	69	13.48	−10.46
2015	3.606	123	121	72	2.5	58	2.5	71	14.84	−9.68
2016	3.664	133	119	45	2.8	86	2.7	85	15.75	−8.88
2017	3.642	140	131	47	2.5	62	2.4	68	15.49	−8.57
2018	3.633	127	123	38	2.5	61	3.0	115	15.01	−10.45
2019	3.641	142	128	25	2.8	84	2.9	120	15.28	−14.09
2020	3.657	150	131	78	2.5	79	2.3	56	14.9	−6.88
2021	3.577	190	152	42	2.6	65	2.8	95	15.2	−14.22
2022	3.65	137	131	50	2.8	91	2.6	71	13.62	−9.54

References

1. Sherstyankin, P.; Alekseev, S.; Abramov, A.; Stavrov, K.G.; De Batist, M.; Hus, R.; Canals, M.; Casamor, J.L. Computer-based bathymetric map of Lake Baikal. *Dokl. Earth Sci.* **2006**, *408*, 564–569. [CrossRef]
2. Timoshkin, O.A.; Sitnikova, T.Y.; Rusinek, O.; Pronin, N.; Proviz, V. *Index of Animal Species Inhabiting Lake Baikal and Its Catchment Area*; Nauka: Novosibirsk, Russia, 2001; Volume 1, p. 832.
3. Galazii, G.I. *Baikal in Questions and Answers*; Forward Ltd.: London, UK , 2012; p. 159.
4. Shimaraev, M.N.; Verbolov, V.I.; Granin, N.; Sherstyankin, P.P. *Physical Limnology of Lake Baikal: A Review*; BICER, Baikal International Center for Ecological Research: Okayama, Japan; Irkutsk, Russia, 1994.
5. Vereshchagin, G. Some data on Baikal deep water regime near Marituy. *Proc. Comm. Lake Baikal Study* **1927**, *2*, 77–138. (In Russian)
6. Shimaraev, M.; Granin, N. On the question of stratification and the mechanism of convection in Baikal. *Dokl. Earth Sci.* **1991**, *321*, 381–385.
7. Sherstyankin, P.; Kuimova, L.; Potemkin, V. Temperature of maximal density and thermobaric properties of deep fresh water: Evidence from Lake Baikal. *Dokl. Earth Sci.* 2000, *375*, 318–1322.
8. Bouffard, D.; Wüest, A. Convection in Lakes. *Annu. Rev. Fluid Mech.* **2019**, *51*, 189–215. [CrossRef]
9. Eklund, H. Stability of Lakes near the Temperature of Maximum Density. *Science* **1965**, *149*, 632–633. [CrossRef] [PubMed]
10. Rzheplinsky, G.V.; Sorokina, A.I. *Atlas of Wave and Wind Action in Lake Baikal*; Gidrometeoizdat: Leningrad, Russia, 1977; p. 118. (In Russian)
11. Weiss, R.; Carmack, E.; Koropalov, V. Deep-water renewal and biological production in Lake Baikal. *Nature* **1991**, *349*, 665–669. [CrossRef]
12. Shimaraev, M.; Granin, N.; Zhdanov, A. Deep ventilation of Lake Baikal due to spring thermal bars. *Limnol. Oceanogr.* **1993**, *38*, 1068–1072. [CrossRef]
13. Hohmann, R.; Kipfer, R.; Peeters, F.; Piepke, G.; Imboden, D.; Shimaraev, M. Processes of deep-water renewal in Lake Baikal. *Limnol. Oceanogr.* **1997**, *42*, 841–855. [CrossRef]
14. Shimaraev, M.; Domysheva, V.; Gnatovskii, R.Y.; Blinov, V.; Sakirko, M. The influence of deep convection on aeration of the bottom zone in Baikal. *Geogr. Nat. Resour.* **2016**, *37*, 212–219. [CrossRef]
15. Tsimitri, C.; Rockel, B.; Wuest, A.; Budnev, N.; Sturm, M.; Schmid, M. Drivers of deep water renewal events observed over 13 years in the South Basin of Lake Baikal. *J. Geophys. Res. Oceans* **2015**, *120*. [CrossRef]
16. Piccolroaz, S.; Toffolon, M. Deep water renewal in Lake Baikal: A model for long-term analyses. *J. Geophys. Res. Oceans* **2013**, *118*, 6717–6733. [CrossRef]

17. Schmid, M.; Budnev, N.; Granin, N.G.; Sturm, M.; Schurter, M.; Wüest, A. Lake Baikal deepwater renewal mystery solved. *Geophys. Res. Lett.* **2008**, *35* . [CrossRef]

18. Wuest, A.; Ravens, T.; Granin, N.; Kocsis, O.; Schurter, M.; Sturm, M. Cold Intrusions in Lake Baikal: Direct Observational Evidence for Deep-Water Renewal. *Limnol. Oceanogr.* **2005**, *50*, 184. [CrossRef]

19. Farmer, D.; Carmack, E. Wind Mixing and Restratification in a Lake near the Temperature of Maximum Density. *J. Phys. Oceanogr.* **1981**, *11*, 1516–1533. [CrossRef]

20. Carmack, E.; Vagle, S. Thermobaric Processes Both Drive and Constrain Seasonal Ventilation in Deep Great Slave Lake, Canada. *J. Geophys. Res. Earth Surf.* **2021**, *126*, e2021JF006288. [CrossRef]

21. Crawford, G.; Collier, R. Long-term observations of deepwater renewal in Crater Lake, Oregon. *Hydrobiologia* **2007**, *574*, 47–68. [CrossRef]

22. Boehrer, B.; Fukuyama, R.; Chikita, K.; Kikukawa, H. Deep water stratification in deep caldera lakes Ikeda, Towada, Tazawa, Kuttara, Toya and Shikotsu. *Limnology* **2009**, *10*, 17–24. [CrossRef]

23. Johnson, L. Temperature of Maximum Density of Fresh Water and its Effect on Circulation in Great Bear Lake. *J. Fish. Res. Board Can.* **1966**, *23*, 963–973. [CrossRef]

24. Vereshchagin, G. The main features of the vertical distribution of water mass dynamics in Baikal. In *Academician V.I. Vernadsky to the 50th Anniversary of Scientific and Pedagogical Activity*; Nauka: Moscow, Russia, 1936; pp. 1207–1230.

25. Verbolov, V. Currents and water exchange in Lake Baikal. *Water Resour.* **1996**, *23*, 381–391.

26. Irkutsk Center for Remote Sensing. Available online: http://sputnik.irk.ru/ (accessed on 10 December 2023).

27. Budnev, N.M.; Wuest, A.; Lovtsov, S.V.; Parfenov, J.V.; Rubstov, V.J.; Rastegin, A.E.; Shturm, M.; Shurter, M.V. The hydrophysical processes in the south Baikal from the point of view of long-term temperature monitoring data. In Proceedings of the Fourth Vereshchagin Baikal Conference, Irkutsk, Russia, 26 September–1 October 2005; Institute of Geography SB RAS Publishers: Irkutsk, Russia, 2005; pp. 24–25.

28. Lovtsov, S.V.; Parfenov, Y.V.; Rastegin, A.E.; Rubtsov, V.Y.; Chensky, A.G. Large scale temperature perturbations and inner waves in the Lake Baikal. In Proceedings of the Baikal School for Young Researchers on the Astrophysics and Microworld Physics (BSYPH 98), Irkutsk, Russia, 11–17 October 1998; pp. 279–285.

29. Zhdanov, A.A.; Gnatovskii, R.Y.; Granin, N.G.; Blinov, V.V.; Aslamov, I.A.; Kozlov, V. Variations of under-ice currents in Southern Baikal by data of 2012–2016. *Water Resour.* **2017**, *44*, 442–452. [CrossRef]

30. Muñoz Sabater, J.; Dutra, E.; Agusti-Panareda, A.; Albergel, C.; Arduini, G.; Balsamo, G.; Boussetta, S.; Choulga, M.; Harrigan, S.; Hersbach, H.; et al. ERA5-Land: A state-of-the-art global reanalysis dataset for land applications. *Earth Syst. Sci. Data* **2021**, *13*, 4349–4383. [CrossRef]

31. Imboden, D.; Wuest, A. Mixing Mechanisms in Lakes. In *Physics and Chemistry of Lakes*; Springer: Berlin/Heidelberg, Germany, 1995; pp. 83–138. [CrossRef]

32. Guseva, S.; Armani, F.; Desai, A.; Dias, N.; Friborg, T.; Iwata, H.; Jansen, J.; Lükő, G.; Mammarella, I.; Repina, I.; et al. Bulk Transfer Coefficients Estimated from Eddy-Covariance Measurements over Lakes and Reservoirs. *J. Geophys. Res. Atmos.* **2023**, *128*, e2022JD037219. [CrossRef]

33. Picard, A.; Davis, R.; Gläser, M.; Fujii, K. Revised formula for the density of moist air (CIPM-2007). *Metrologia* **2008**, *45*, 149. [CrossRef]

34. Mantel, N. The detection of disease clustering and a generalized regression approach. *Cancer Res.* **1967**, *27*, 209–220. [PubMed]

35. Dixon, P. VEGAN, a package of R functions for community ecology. *J. Veg. Sci.* **2003**, *14*, 927–930. [CrossRef]

36. Kassambara, A. *Practical Guide to Principal Component Methods in R: PCA, M (CA), FAMD, MFA, HCPC, Factoextra*; 2017; Volume 2. Available online: http://www.sthda.com/english/wiki/practical-guide-to-principal-component-methods-in-r (accessed on 1 December 2023).

37. Livingstone, D. Ice break-up on southern Lake Baikal and its relationship to local and regional air temperatures in Siberia and to the North Atlantic Oscillation. *Limnol. Oceanogr.* **1999**, *44*, 1486–1497. [CrossRef]

38. Magnuson, J.J.; Robertson, D.M.; Benson, B.J.; Wynne, R.H.; Livingstone, D.; Arai, T.; Assel, R.A.; Barry, R.J.; Card, V.; Kuusisto, E.; et al. Historical Trends in Lake and River Ice Cover in the Northern Hemisphere. *Science* **2000**, *289*, 1743–1746. [CrossRef]

39. Shimaraev, M.; Kuimova, L.; Sinyukovich, V.; Tsekhanovskii, V. Climate and hydrological processes in Lake Baikal in the 20th century. *Russ. Meteorol. Hydrol.* **2002**, *3*, 52–58.

40. Todd, M.; Mackay, A. Large-Scale Climatic Controls on Lake Baikal Ice Cover. *J. Clim.* **2003**, *16*, 3186–3199. [CrossRef]

41. Troitskaya, E.; Shimaraev, M.; Tsekhanovsky, V. Long-term changes in water surface temperature in Baikal. *Geogr. Prir. Resur. [Geogr. Nat. Resour.]* **2003**, *2*, 47–50.

42. Kouraev, A.; Semovski, S.; Shimaraev, M.; Mognard, N.; Legrésy, B.; Rémy, F. The ice regime of Lake Baikal from historical and satellite data: Relationship to air temperature, dynamical, and other factors. *Limnol. Oceanogr.* **2007**, *52*, 1268–1286. [CrossRef]

43. Katz, S.; Hampton, S.; Izmest'eva, L.; Moore, M. Influence of Long-Distance Climate Teleconnection on Seasonality of Water Temperature in the World's Largest Lake—Lake Baikal, Siberia. *PLoS ONE* **2011**, *6*, e14688. [CrossRef] [PubMed]

44. Goldman, C.; Kumagai, M.; Robarts, R. *Climatic Change and Global Warming of Inland Waters: Impacts and Mitigation for Ecosystems and Societies*; John Wiley & Sons, Ltd.: Hoboken, NJ, USA, 2012. [CrossRef]

45. Sizova, L.; Kuimova, L.; Shimaraev, M. Influence of the atmospheric circulation on ice-thermal processes on Baikal during 1950–2010. *Geogr. Nat. Resour.* **2013**, *34*, 158–165. [CrossRef]

46. O'Reilly, C.M.; Sharma, S.; Gray, D.; Hampton, S.; Read, J.S.; Rowley, R.J.; Schneider, P.; Lenters, J.D.; McIntyre, P.B.; Kraemer, B.M.; et al. Rapid and highly variable warming of lake surface waters around the globe. *Geophys. Res. Lett.* **2015**, *42*, 10773–10781. [CrossRef]

47. Shimaraev, M.; Troitskaya, E. Current trends in upper water layer temperature in coastal zones of Baikal. *Geogr. Nat. Resour.* **2018**, *39*, 349–357. [CrossRef]

48. Shimaraev, M.; Troitskaya, E.; Gnatovskii, R.Y. Modern climate changes and deep water temperature of Lake Baikal. *Dokl. Earth Sci.* **2009**, *427*, 804–808. [CrossRef]

49. Troitskaya, E.; Budnev, N.; Shimaraev, M. Changes in the heat content of water column in the slope area of the southern basin of Lake Baikal in the 21st Century. *Water* **2022**, *14*, 348. [CrossRef]

50. Bulygina, O.N.; Korshunova, N.N.; Razuvaev, V.N. Changes in the wind regime over Russia in the last decades. *Proc. Main Geophys. Obs. Named After A. I. Voeikov* **2013**, *568* , 156–172.

51. Coumou, D.; Lehmann, J.; Beckmann, J. The weakening summer circulation in the Northern Hemisphere mid-latitudes. *Science* **2015**, *348*, 324–327. [CrossRef]

52. Verbolov, V.I.; Sokolnikov, V.M.; Shimaraev, M.N. *Hydrometeorological Regime and Heat Balance of Lake Baikal*; Nauka: Leningrad, Russia; Moscow, Russia, 1965; p. 374.

53. Shimaraev, M.N. *The Elements of the Thermal Regime of Lake Baikal*; Nauka: Novosibirsk, Russia, 1977; p. 149.

54. Shimaraev, M.; Granin, N.; Kuimova, L. Practice of reconstruction of Baikal hydrophysical conditions in the Late Pleistocene and Holocene. *Geol. Geofiz.* **1995**, 97–102.

55. Ravens, T.; Kocsis, O.; Wuest, A.; Granin, N. Small-scale turbulence and vertical mixing in Lake Baikal. *Limnol. Oceanogr.* **2000**, *45*, 159–173. [CrossRef]